LoRaWAN Analysis under Unsaturated Traffic, Orthogonal and non-Orthogonal Spreading Factor Conditions

Inès El Korbi*, Yacine Ghamri-Doudane † and Leila Azouz Saidane*
* National School of Computer Science, CRISTAL Lab, University of Manouba, 2010 Tunisia
† L3i Lab, University of La Rochelle, Av. Michel Crépeau, 17042, La Rochelle CEDEX 1, France
ines.korbi@ensi.rnu.tn, yacine.ghamri@univ-lr.fr, leila.saidane@ensi-uma.tn

***Abstract*—LoRaWAN is the new transmission protocol for Low-Power Wide Areas (LPWA) networks. In addition to long range communications, one of the most solid arguments in favour of the LoRaWAN technology is its ability to operate at orthogonal spreading factors (SFs). This enables simultaneous transmissions at different data rates on the same frequency channel. But Recently, it has been shown that transmissions at different SFs are not perfectly orthogonal which generates cross-SF interferences (i.e. interferences between different spreading factors' transmissions). Therefore, we propose here an analytical model of a single cell LoRaWAN under unsaturated traffic, duty cycle and multi-channel deployment conditions. The model considers both perfect and imperfect SF orthogonality scenarios. The network performance are then derived in terms of achievable throughput at the gateway as a function of the offered load, the number of received packets per device and the percentage of successful transmissions. All the Results show that if spreading factors are assumed to be orthogonal, the capture effect improves the network performance in comparison with the theoretical pure Aloha access scheme. Whereas, the consideration of imperfect SF orthogonality revises the LoRaWAN performance downward.**

I. Introduction

In the past few years Low-Power Wide-Area (LPWA) networks were proposed as a potential communication technology for the IoT traffic transportation from sensors/objects to the appropriate gateways. In the opposite to multi-hop communications where the forwarding process is complex and requires high energy consumption, with LPWA, nodes can directly reach the wired infrastructure at a very low transmission power. In this context, LoRaWAN [1], a new LPWA wireless communication protocol has raised much interest given its deployment ease and its open aspects (open specifications and operation in unlicensed ISM bands). LoRaWAN is based on the LoRa modulation [2] largely inspired from the CSS (Chirp Spread Spectrum) modulation. The chirp spreading mechanism allows high resistance to interferences, thus a good signal reception miles away from the emitters. Despite the efficiency of the LoRa modulation, LoRaWAN operates in very narrow ISM bands (EU 863-870 MHz, US 902-928 MHz). To increase its throughput LoRa adopts the spreading factors' mechanism. With spreading factors, several signals can be sent on the same frequency band at different data rates. Thus, as spreading factors increase, the receiver's sensitivity (its ability to pick up the required level of radio signals) increases too at the expense of bit rates' decrease. Theoretically, transmissions at different spreading factors are perfectly orthogonal and can be simultaneously decoded by the gateway. But very recent studies have shown that in reality, spreading factors are not perfectly orthogonal [3], [4], [5]. Hence, a correct signal reception at a given spreading factor is conditioned by the absence of all cross SF-interferences (i.e. interferences between transmissions at different spreading factors). Works that tackled the imperfect SF orthogonality in LoRaWAN either analytically evaluated LoRaWAN saturation throughput while considering a rough estimation of cross-SF interferences [5], or conducted real experiments to illustrate the imperfect SF orthogonality phenomenon [3], [4]. Other works, evaluated the LoRaWAN scalability through simulations while considering real cross-SF interference thresholds [6], [7].

In the hereby paper, we propose a new LoRaWAN analysis that aims to compare the network performance when either orthogonal or non-orthogonal spreading factors' deployment scenarios are considered. The analysis will be conducted under unsaturated traffic, duty cycle and multi-channel conditions. The performance results will be derived in terms of achievable gateway throughput as a function of the offered load per end device, the number of received packets per device and the percentage of successful transmissions. The rest of the paper will be organized as follows. In the next section, we review the LoRa and LoRaWAN fundamental concepts. Then, we discuss the works related to the performance evaluation of LoRa networks either analytically, through simulations or testbeds. In Section III, we present the system model we adopt at the physical and the network layers. In Section IV, we derive the LoRaWAN analysis in both orthogonal and non-orthogonal SF conditions. Section V will be dedicated to the discussion of the LoRaWAN performance results. Finally, we conclude the paper and present future directions in Section VI.

II. Background and Related Work

A. LoRa and LoRaWAN overview

Today LoRaWAN [1] stands as one of the most powerful LPWA solutions dedicated to IoT communications. Its owes

978-1-5386-7659-2/18/$31.00

its notoriety to many factors: free standard (open LoRaWAN specifications), free access on the ISM bands, certified hardware, etc. In the following we present the main LoRaWAN aspects at the physical and the network layers as specified by the LoRa Alliance[1].

1) The LoRaWAN physical layer: LoRaWAN uses the LoRa modulation [2] at the physical layer which is a variation of the Chirp Spread Spectrum (CSS) modulation. CSS consists in generating chirp signals that continuously vary (continuously increasing or continuously decreasing) in frequencies. Each chirp/symbol will be in charge of transmitting a fixed number of bits. The number of bits per symbol is called Spreading factor (SF). In LoRa, SFs vary from 7 to 12. For instance, as spreading factors increase, the receiver's sensitivity increases too and henceforth does the communication range. In the opposite, data bit rates drop down and transmission durations, referred as Times on Air (ToA) become longer. The relationship between spreading factors (SFs), date rates (R_b) and modulation bandwidth (BW) is given by:

$$R_b = SF * \frac{BW}{2^{SF}} \quad (1)$$

LoRa transceivers can operate in bandwidth ranges from 137 MHz to 1020 MHz. They are, however, often deployed in the ISM bands 868 MHz for Europe and 915 MHz for USA. In the European region, for instance, LoRa Alliance states that each end device must implement the three default channels: 868.10, 868.30 and 868.50 MHz, each of 125 kHz bandwidth. On each channel, data rates from DR_0 to DR_5 must be implemented (cf. Table I). Moreover, according to the ETSI[2] regulations in Europe, the maximum output power on each device is +14 dBm and the duty-cycle limit is set to 1% for the three mandatory channels. LoRa modems also provide, through Coding Rates (CRs), a FEC mechanism to enhance protection against bit corruption. Coding Rates vary from 4/5 to 4/8 (respectively denoted as CR = 1 to CR = 4).

TABLE I
DATA RATES AND RELATED CONFIGURATION (EU. 863-870 MHZ)

DR_i	SF	Sensitivity	BR (bits/s)	SNR (dB)
0	12	-137	250	-7.5
1	11	-134.5	440	-10
2	10	-132	980	-12.5
3	9	-129	1760	-15
4	8	-126	3125	-17.5
5	7	-123	5470	-20

2) The LoRaWAN network layer: LoRaWAN is the communication protocol defined by the LoRa Alliance on the top of the LoRa physical layer. LoRaWAN is a star based topology where thousands of objects (sensors or actuators) can directly send their data to a gateway using LoRa modulation. This latter will be in charge of forwarding, through backhaul, the collected data to a network server for processing (c.f. Figure 1).

At the MAC layer, LoRaWAN defines three bi-directional operation classes. The class A, known as the basic service class, is supported by all devices that decide themselves when to transmit using a pure Aloha protocol. After sending message to the gateway (uplink), a device opens two receive windows, one for the acknowledgments and the other for the downlink traffic. With class B, additional downlink traffic is enabled to allow gateways sending beacon frames at regular intervals. In class C, devices can continuously receive frames, except when transmitting. At the MAC layer, LoRaWAN defines six type of messages that aim to join the LoRa network, send/receive unconfirmed data or send/receive confirmed data. To ensure the communication security, LoRaWAN provides end-to-end encryption and data integrity.

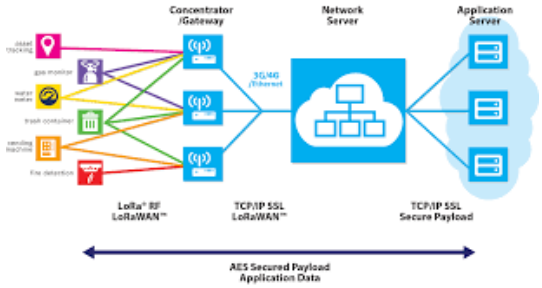

Figure 1. LoRaWAN Architecture (Semtech picture courtesy)

B. Related work

Early works on LoRa/LoRaWAN were interested in evaluating the impact of the LoRa physical parameters (SF, CR, bandwidth, etc.) on the network performance through measurement campaigns, real experiments and testbeds [8], [9], [10]. Thereafter, several works tackled more global issues in LoRaWAN such as scalability [11], the network capacity in terms of the number of supported end devices [12], the energy consumption [13] or the delay analysis [14]. One of the most interesting studies in this context is [15] that derives the class A LoRaWAN throughput with pure Aloha access scheme. The authors in [15] proposed a model that captures major LoRaWAN aspects such as duty cycle, multi-channel access or the time on air. The results showed that the network performance mainly depend on the monitored application traffic characteristics. However, the model in [15] only considers the LoRaWAN characteristics at both medium access and network layers. Whereas, the physical layer properties were completely ignored (interferences between signals transmitted at the same or different SFs). For instance, in LoRaWAN specification [1] and early works [8], [11], [12], it was considered that data transmissions on each spreading factor are orthogonal which allows the gateway to correctly decode traffic coming from different nodes on the same frequency band.

But very recent results [16], [3], [5] have shown through real experiments and numerical analysis of the LoRa modulation

[1]A Consortium of telecommunications operators, electronic companies and research institutions that adopted the LoRaWAN technology https://lora-alliance.org/

[2]The European Telecommunications Standards Institute

that a signal transmitted by an end device to the gateway may suffer two kinds of disruption leading to its premature outage. This disruption can be either caused by co-SF interferences (i.e. interferences coming from transmissions using the same spreading factor) or cross-SF interferences (i.e. interferences coming from transmissions using different spreading factors). Thus, to be correctly decoded, a packet sent at a given SF should respect Signal-to Interference-plus-Noise-Ratio (SINR) margins (in db units) with all other spreading factors as illustrated in Table II [7], [17].

TABLE II
SINR THRESHOLDS FOR ALL SF PAIRS

Desired SINR	7	8	9	10	11	12
7	6	-16	-18	-19	-19	-20
8	-24	6	-20	-22	-22	-22
9	-27	-27	6	-23	-25	-25
10	-30	-30	-30	6	-26	-28
11	-33	-33	-33	-33	6	-29
12	-36	-36	-36	-36	-36	6

Subsequently, new works integrate this result in their evaluation of the LoRa network. Thus, [18] developed a simulation model where co/cross-SF interferences were considered to derive the impact of the IoT traffic on the LoRaWAN performance. In [4], the authors thoroughly examined the SF orthogonality aspect and demonstrated the efficiency of using different SFs in pipelined multihop LoRaWANs. [5] proposes an analytical model of the LoRaWAN saturation throughput under orthogonal and non orthogonal SF conditions. Despite its novelty, the model presented in [5] only focused on the saturation throughput derivation while ignoring how IoT applications, with their different characteristics, impact this network performance. Moreover, throughput expressions were derived using slotted Aloha access scheme whereas class A users contend for the medium through pure Aloha. The usage of a slotted access scheme requires a regular gateway synchronization [19] which is not always possible in class A LoRaWAN where most of the traffic is unacknowledged. In addition, the model does not integrate duty cycle and multi-channel properties. Finally, in the case of imperfect SF orthogonality, mutuel spreading factors' SINR thresholds were not considered individually and only rough estimations of cross-SF SINR margins were integrated for the model evaluation.

C. Main contributions

From the above discussion of the LoRaWAN state of art and related work, we can clearly state the paper contributions as follows:

1) We propose here an analytical model of a single cell LoRaWAN to derive its performance under orthogonal and non-orthogonal spreading factors' transmissions. The performance will be evaluated in terms of the achievable throughput at the gateway, the number of received packets per end device and the percentage of successful transmissions.
2) The analysis will be conducted under unsaturated traffic conditions to illustrate how IoT applications' characteristics impact the network performance.
3) The pure Aloha access scheme will be considered at the network layer [1]. In the opposite to slotted Aloha, with pure Aloha transmissions are not synchronized. Thus a tagged packet transmission can be annoyed by early or late transmitters [20] which significantly deviates the network performance.
4) Both duty cycle and multi-channel aspects will be considered in the analytical model.
5) In the case of non-orthogonal SFs, the network performance parameters will be derived given exact values of mutual SINR thresholds.

III. SYSTEM DESCRIPTION

In this paper, we focus on the LoRaWAN evaluation under unsaturated traffic conditions for two case studies: orthogonal and non-orthogonal spreading factors' transmissions. Thus, depending on the SF orthogonality considerations (perfect or imperfect orthogonality), a signal at the gateway will be correctly received if one or more of the three following capture conditions are met:

- **Condition 1***:* The signal power received at a given spreading factor SF_i must be above the signal to noise ratio (SNR) required for that spreading factor as shown in Table I.
- **Condition 2***:* A signal transmitted at a spreading factor SF_i is correctly captured if the co-SF $SINR(i,i)$ is higher than a given threshold θ_{ii} (i.e. the transmitted signal can not be disturbed by other transmissions using the same SF).
- **Condition 3***:* A signal transmitted at a spreading factor SF_i is correctly captured if for each SF_j, $j \neq i$, we have $SINR(i,j)$ is higher than θ_{ij} (i.e. the transmitted signal can not be disturbed by any other transmission using any other spreading factor SF_j).

Therefore, we first define the radio propagation and the network models we adopt in our study.

A. Propagation model and physical layer parameters

According to the above description of the LoRa modulation scheme in Section II-A1, we can state the following assumptions related to the model we adopt at the physical layer:

1) The end devices are all equipped with LoRa transceivers and transmit at a fixed power P_0.
2) We assume that the transmitted signals are subject to path loss, shadowing and fading effects where:
   - follows from the Friis transmission equation [16], the path loss attenuation function $g(r) = f_c/(4\pi r)^{\alpha}$, where f_c is the carrier frequency, α is the path loss exponent ($\alpha = 2.7$ in sub-urban environments) and r is the distance (in m) to the gateway.

- the channel gain due to fading between an end-device and the gateway is given by $|h_0|^2$. We have $|h_0|^2 \backsim \mathcal{N}(0,1)$ for the Rayleigh fading [16], [5].
- the shadowing adds zero-mean AWGN to the path loss with noise variance:

$$\sigma^2 = -174 + NF + 10log(BW)\ [dBm], \quad (2)$$

where BW is the signal bandwidth. NF is the receiver's noise figure that can be considered to have a value of 6 dB in the hardware implementations [17].

3) In the LoRa network, end devices can transmit at a given spreading factor SF_i belonging to the set $S = \{SF_1, ..., SF_K\}$ of spreading factors $(K = 6)$. We have: $SF_1 = 7$ and $SF_K = 12$.
Thus, given assumptions 1 and 2 and according to [5], a signal transmitted using SF_i can be received at a maximum distance l_i from the emitter:

$$l_i = \left(\frac{P_0 f_c}{(4\pi)^\alpha \psi_i}\right)^{\frac{1}{\alpha}} \quad (3)$$

where ψ_i is the receiver's sensitivity at SF_i (cf. Table I).

4) Given the Rayleigh-faded envelope of the transmitted signal, the instantaneous signal to noise ratio (SNR) γ_0 of an end device ED_0 at the receiver situated at a distance r_0 from ED_0 is exponentially distributed as [21]:

$$f_{\Gamma_0}(\gamma_0) = \frac{1}{\overline{\gamma_0}} \exp\left(\frac{\gamma_0}{\overline{\gamma_0}}\right) \quad (4)$$

where $\overline{\gamma_0}$ is the local-mean SNR of the transmitted signal at the receiver:

$$\overline{\gamma_0} = \frac{P_0 f_c}{(4\pi r_0)^\alpha \sigma^2} = \beta r_0^{-\alpha} \quad (5)$$

$\beta = \frac{P_0 f_c}{(4\pi)^\alpha \sigma^2}$ is constant and identical for all the end devices.

B. Network model

Now that we have set the physical layer parameters, we focus here on the network model and consider the following assumptions:

1) The LoRa network is a single cell area of radius R where N end devices are uniformly distributed and transmit data to a single gateway G_0 placed at the cell center and able to receive up to 8 signals in parallel [1]. R corresponds to the highest spreading factor's ($SF_6 = 12$) distance threshold. According to Equation (3), we have: $R = l_6$ and G_0 is placed at the radius $l_0 = 0$.
2) Spreading factors are assigned to end devices according to their distances to the gateway. Thus, if a node ED_0 is situated at a distance r_0 from the gateway such as $l_{i-1} \leq r_0 \leq l_i$, it will be assigned the spreading factor SF_i (cf. Figure 2). l_{i-1} and l_i respectively correspond to SF_{i-1} and SF_i distance thresholds given by Equation (3).
3) End devices have the same packet generation rate λ and the same packet size L.

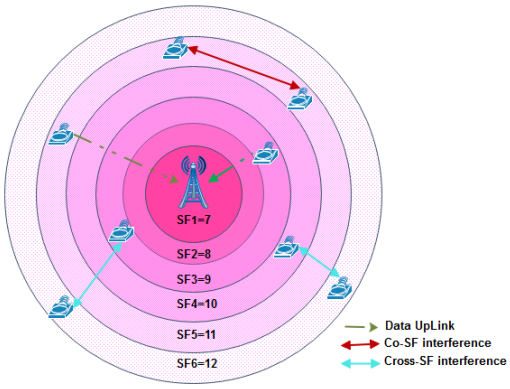

Figure 2. LoRaWAN system setup: distance based SF allocation

4) Each end device implements M frequency channels. According to the LoRa specification, the minimum M value is 3, which corresponds to the three mandatory frequency channels in the EU 868 MHz unlicensed band $[868.1, 868.3, 868.5]$ MHz. In all these bands the duty cycle limit is fixed to $d = 1\%$.

From the above assumptions, we can derive the following notations:

- The time on air (ToA) for each SF_i is evaluated as follows:

$$ToA_i = \frac{2^{SF_i}}{BW}\left(((NP+4.25) + SW + \max\left(ceil\left[\frac{8\,PL - 4\,SF_i + 28 + 16\,CRC - 20\,IH}{4(SF_i - 2\,DE)}\right](CR+4), 0\right)\right)\right) \quad (6)$$

where:
- BW is the channel's bandwidth.
- NP is the number of preamble symbols (NP=8 bytes) and SW is the length of synchronization word (SW=8 bits).
- CRC and IH: specify the presence of CRC and physical header for the packet. We have, CRC=0 and IH=1 for the uplink traffic.
- DE : indicates the use of data rate optimization ($DE = 1$ for DR_0 and DR_1, i.e. $SF_6 = 12$ and $SF_5 = 11$).
- CR : Coding rate. $CR = 1$ corresponds to $4/5$ coding rate.
- PL: the number of the physical layer payload bytes.

$$PL = 12 + FHDR_{OPTS} + FPort + FRMPayload \quad (7)$$

where $FHDR_{OPTS}$ is the length of the optional frame header field carrying MAC commands, $FPort = 1$ is the application specific port. $FRMPayload$ is the size in bytes of the application payload.

- Let λ_i^M, be the packet generation rate per channel of a given end device transmitting at the spreading factor SF_i.

$$\lambda_i^M = \min\left(\frac{\lambda}{M}, \frac{d}{ToA_i}\right) \quad (8)$$

where $\frac{\lambda}{M}$ is the packet generation rate per channel per end device and d is the duty cycle limit per channel and is identical for all the channels [15].

- We define by N_i, the number of nodes using the spreading factor SF_i, i.e. the end devices situated in the annulus defined by the smaller and the larger radii l_{i-1} and l_i. From assumptions 1 and 2, we have :

$$N_i = N \int_{l_{i-1}}^{l_i} \frac{2r}{R^2} dr$$

where R is the network communication radius.

IV. LoRaWAN Performance Analysis

This section is dedicated to the LoRaWAN performance analysis. We first evaluate the throughput metric achieved at the gateway G_0. In reference to [15] and under the assumption of pure Aloha access, the LoRaWAN capacity at the MAC layer can be roughly calculated as the superposition of independent ALOHA-based networks (one independent network for each channel and for each SF). In this context, the expression of the throughput B can be evaluated as:

$$B = M \sum_{i=1}^{K} B_i^M = M \sum_{i=1}^{K} N_i \rho_i^M e^{-2N_i \rho_i^M} \tag{9}$$

where B_i^M is the per channel throughput achieved by all the nodes transmitting at SF_i. ρ_i^M is the per channel offered load of an end device transmitting at SF_i.

$$\rho_i^M = \lambda_i^M ToA_i \tag{10}$$

The expression of B in Equation (9) assumes that two signals with the same SF obviously collide at G_0. But concurrent transmissions at different SFs could be perfectly decoded.

In reality, and in accordance with the related work discussion in Section II-B, the phenomena that occur at the physical layer deviate the throughput actually achieved at G_0. Indeed, the gateway could perfectly decode two signals transmitted with the same SF_i if the SINR between these two signals is above a certain threshold. On the other hand, signals transmitted at other SF_j could preclude the correct reception of the SF_i signal if the mutuel (SF_i, SF_j) SINR margin is below a given value. In the following we derive the correct throughput expressions in both perfect and imperfect SF orthogonality situations.

A. Case Study 1: Orthogonal Spreading Factors conditions

In this first case of study, we are in perfect SF orthogonality conditions, i.e. the signals coming from two different SFs do not interfere with each other. Thus, the correct reception of a signal transmitted by an end device ED_0^i (using SF_i and placed at a distance r_i^0 from G_0) is subject to the capture conditions 1 and 2 as defined in Section III. The condition 1 can be rewritten as:

$$\gamma_i^0 \geq \gamma_i^{th} \tag{11}$$

where γ_i^0 is the node ED_0^i SNR as defined in Section III-A and γ_i^{th} is the SF_i SNR threshold given in the last column of the Table I.

Given the general SINR expression [7] and using the noise variance normalization, condition 2 can be formulated as [5]:

$$SINR(i,i) = \frac{\gamma_i^0}{\sum_{p=1}^{n_i} \gamma_i^p + 1} \geq \theta_{ii} \tag{12}$$

where γ_i^p is the SNR of the node ED_p^i , interfering with ED_0^i at the same channel and the same SF_i. n_i is the number of interfering packets at SF_i and θ_{ii} is the *co-*SF_i SINR threshold as defined in Table II.

According to [22], [20] we can express B_i^M, the per channel SF_i throughput as:

$$B_i^M = N_i \rho_i^M \sum_{n_i=0}^{N_i-1} P\left[Capture\ ED_0^i / n_i\right] \Pr\left[n_i\right] \tag{13}$$

where n_i is the number of interferers at SF_i, $P\left[Capture\ ED_0^i/n_i\right]$ is the probability that the ED_0^i signal is correctly captured at G_0 given n_i interferers.

Let $f_{\Gamma_i}(\gamma)$ (resp. $F_{\Gamma_i}(\gamma)$) be the *pdf* (resp. the complementary density function (*cdf*)) of the SF_i SNR at G_0. We also define Z_i, the random variable corresponding to the SINR observed at G_0 by a packet transmitted at SF_i, which *pdf* is f_{Z_i} and *cdf* is F_{Z_i}. If $n_i = 0$, then the probability of capture is conditioned by the fulfillment of only condition 1. Otherwise, if $n_i > 0$, the satisfaction of condition 2 implies the satisfaction of condition 1 too (We said that condition 2 is dominant on condition 1) [5]. Thus:

$$\begin{aligned} B_i^M = N_i \rho_i^M e^{-2N_i \rho_i^M} \big[& F_{\Gamma_i}(\gamma_i^{th}) \\ & + \sum_{n_i=1}^{N_i-1} \frac{\left(2N_i \rho_i^M\right)^{n_i}}{n_i!} F_{Z_i/n}(\theta_{ii}) \big) \big] \end{aligned} \tag{14}$$

If we focus on a particular end device ED_0^i placed at a distance r_i^0 from G_0, the *pdf* of ED_0^i SNR denoted by $f_{\Gamma_i^0}(\gamma_i^0)$ is given by Equation (4). Moreover, as nodes using SF_i are placed in the annulus ϑ_i defined by radii l_i and l_{i-1}, the *pdf* of the distance r_i^0 to the gateway of a randomly chosen node ED_0^i within the annulus ϑ_i is $f_{\vartheta_i}(r_i^0) = \frac{2r_i^0}{|\vartheta_i|}$, where $|\vartheta_i| = (l_i^2 - l_{i-1}^2)$ [16]. Therefore, according to Equation 11 and in reference to [21], we get:

$$\begin{aligned} F_{\Gamma_i}(\gamma_i^{th}) &= \int_{r_{i=0}^0}^{\infty} \left[\int_{\gamma=\gamma_i^{th}}^{\infty} f_{\Gamma_i^0}(\gamma_i^0) d\gamma_i^0 \right] f_{\vartheta_i}(r_i^0) dr_i^0 \\ &= \int_{r_i^0=l_{i-1}}^{l_i} \exp\left(\frac{\gamma_i^{th} \left(r_i^0\right)^{\alpha}}{\beta} \right) \frac{2r_i^0}{|\vartheta_i|} dr_i^0 \end{aligned} \tag{15}$$

Now, we go through the evaluation of $f_{Z_i/n_i}(z)$, the *pdf* of the random variable Z_i given the presence of n_i interferers at SF_i. For pure Aloha, the transmission of a packet P_0^i at time instant t_0 by the node ED_0^i can interfere at SF_i either with early transmitters (packets transmitted before t_0) or late transmitters (packets transmitted after t_0). Thus, the vulnerability period of P_0^i corresponds to the time interval $[t_0 - ToA_i, t_0 + ToA_i] = 2 * ToA_i$, where ToA_i is the time on air of the packet P_0^i. Hence, given n_i, the number of

SF_i interferers during time interval $2 * ToA_i$, there are 2^{n_i} possible realizations of early and late interferers during this interval. A realization $r_{n_i}^k = \left[I_{n_i}^k(t_0), I_{n_i}^k(t_1), ..., I_{n_i}^k(t_{n_i})\right]$ is a vector of values $I_{n_i}^k(t_i)$ that correspond to the number of interferers left after the occurrence of the i^{th} event (arrival of late interferer or departure of early interferer). If we denote by j, the maximum number of interferers during time interval $2 * ToA_i$, $\left\lceil \frac{n_i}{2} \right\rceil \leq j \leq n_i$, there will be $C_{n_i}(j)$ realizations among 2^{n_i} where j is the maximum number of interferers during $2 * ToA_i$ [20]. The explicit expression of $C_{n_i}(j)$ is given in Equation (9b) in [20]. Thus:

$$f_{Z_i/n_i}(z) = \frac{1}{2^{n_i}} \sum_{j=\lceil n_i/2 \rceil}^{n_i} C_{n_i}(j) f_{Z_i/n_i,j}(z) \tag{16}$$

Let $\gamma_i^1, \gamma_i^2, ..\gamma_i^j$ be the SNRs of the j packets, respectively situated at positions $r_i^1, r_i^2, ..r_i^j$ from the gateway and interfering with the packet P_0^i, having an SNR γ_i^0 and placed at position r_i^0 from G_0. According to Equation (4), for each $p \in [0, j]$, $f_{\Gamma_i^p}(\gamma_i^p) = \frac{1}{\overline{\gamma_i^p}} \exp(-\frac{\gamma_i^p}{\overline{\gamma_i^p}})$, where $\overline{\gamma_i^p} = \beta \left(r_i^p\right)^{-\alpha}$. Let $W = \sum_{p=1}^{j} \Gamma_i^p$, be the random variable corresponding the sum of the j interfering packets SNRs, whose *pdf* is $f_W(w) = \left[f_{\Gamma_i^1} \circledast ... \circledast f_{\Gamma_i^j}\right](w)$. Therefore, according to [22], we can write:

$$\begin{aligned} &f_{Z_i/n_i,j,r_i^1,r_i^2...r_i^j}(z) \\ &= \int_{w=1}^{\infty} w f_{\Gamma_i^0}(zw) \left[f_{\Gamma_i^1} \circledast ... \circledast f_{\Gamma_i^j}\right](w-1) dw \end{aligned} \tag{17}$$

Using the Fubini theorem in relation with the convolution product [23] and after variable change we obtain:

$$\begin{aligned} &f_{Z_i/n_i,j,r_i^0,r_i^1...r_i^j}(z) = \int_{\gamma_i^0=0}^{\infty} ... \int_{\gamma_i^p=0}^{\infty} f_{\Gamma_i^0}(z(1+\gamma_i^1+...+\gamma_i^j)) \\ &f_{\Gamma_i^1}(\gamma_i^1)...f_{\Gamma_i^j}(\gamma_i^j) d\gamma_i^1 ... d\gamma_i^j \end{aligned} \tag{18}$$

Then, according to [21], [24] and by integrating over $\gamma_i^0, \gamma_i^1, ..\gamma_i^j$, we obtain:

$$F_{Z_i/n_i,j,r_i^0,r_i^1,r_i^2...r_i^j}(z) = \prod_{p=1}^{j} \frac{1}{1 + z\left(\frac{r_i^p}{r_i^0}\right)^{-\alpha}} \exp(\frac{z\left(r_i^0\right)^{\alpha}}{\beta}) \tag{19}$$

As $r_i^0, r_i^1, r_i^2 ... r_i^j$ are identically distributed and by integrating over $r_i^0, r_i^1, r_i^2 ... r_i^j$, we have:

$$F_{Z_i/n_i,j}(z) = \int_{r_i^0=l_{i-1}}^{l_i} \left[I(r_i^0)\right]^j \exp(\frac{z\left(r_i^0\right)^{\alpha}}{\beta}) \frac{2r_i^0}{|\vartheta_i|} dr_i^0 \tag{20}$$

where $I(r_i^0)$ is evaluated as [21]:

$$I(r_i^0) = \int_{r_i^p=l_{i-1}}^{l_i} \frac{2 * r_i^p}{|\vartheta_i|} \frac{dr_i^p}{1 + z\left(\frac{r_i^p}{r_i^0}\right)^{-\alpha}} \tag{21}$$

Finally, by a simple integration of the equation (16), we obtain:

$$\begin{aligned} &F_{Z_i/n_i}(z) = \tfrac{1}{2^{n_i}} \times \\ &\textstyle\sum_{j=\lceil n_i/2 \rceil}^{n_i} C_{n_i}(j) \int_{r_i^0=l_{i-1}}^{l_i} \left[I(r_i^0)\right]^j \exp(\frac{z\left(r_i^0\right)^{\alpha}}{\beta}) \frac{2r_i^0}{|\vartheta_i|} dr_i^0 \end{aligned} \tag{22}$$

Hence, B_i^M is obtained by replacing the expression of $F_{Z_i/n_i}(\theta_{ii})$ given by the equation (22) in the equation (14). The overall throughput achieved at the gateway will be equal to $B = M \sum_{i=1}^{K} B_i^M$.

B. Case Study 2: Non-orthogonal Spreading factors

In this second case of study, we consider that transmissions at different spreading factors interfere with each other, thus precluding from a correct signal reception at the gateway unless the three capture conditions defined in Section III are satisfied. As conditions 1 and 2 were already considered in the computation of the throughput in perfect SF-orthogonality conditions, we focus here on the third condition formulation related to cross-SF interferences. Therefore, for each transmission of an ED_0^i at SF_i, cross-SINR thresholds with each spreading factor SF_j, $j \neq i$ should also be satisfied. Thus, condition 3 becomes:

$$SINR(i,j) = \frac{\gamma_i^0}{\sum_{p=1}^{n_j} \gamma_j^p + 1} \geq \theta_{ij} \tag{23}$$

where n_j is the number of SF_j nodes interfering with ED_0^i. θ_{ij} is the *cross-*$SINR(i,j)$ threshold as defined in Table II. Analogically to Equation (13), we can write B_i^M here as:

$$B_i^M = N_i \rho_i^M \sum_{n_1=0}^{N_1} ... \sum_{n_K=0}^{N_K} P[capture\ ED_0^i\ /_{n_1,...,n_K}] \Pr[n_1, ..., n_K] \tag{24}$$

where $P[capture\ ED_0^i\ /_{n_1,...,n_K}]$ is the probability that a packet transmitted by ED_0^i is correctly captured while $n_1, ..., n_K$ interferers are transmitting at spreading factors $SF_1, ..., SF_K$. Thus, as in the orthogonal SF case, if $(n_1, ..., n_K) = (0, ..., 0)$, only condition 1 applies. Otherwise, conditions 2 and 3 are dominant on condition 1 [5]. Moreover, we assume that $SINR$ thresholds at each spreading factor should be satisfied independently of each other [16], [7]. We, therefore define Z_{ij}, the random variable of the SF_i SINR observed at G_0 in the presence of SF_j interferers, which *pdf* is $f_{Z_{ij}}$ and *cdf* is $F_{Z_{ij}}$. Moreover, if the number of SF_j interferers, $n_j = 0$, then we set $F_{Z_{ij}/n_j} = 1$. Hence:

$$\begin{aligned} B_i^M = N_i \rho_i^M e^{-\sum_{l=1}^{K} N_l \rho_l^M} \Big[&F_{\gamma_i}(\gamma_i^{th}) + \\ &\prod_{l=1}^{K} \left(\sum_{n_l=1,(n_1...n_k)\neq(0...0)}^{N_l'} F_{Z_{il}/n_l}(\theta_{il}) \frac{\left(N_l \rho_l^M\right)^{n_l}}{n_l!} \right) \Big] \end{aligned} \tag{25}$$

where $F_{Z_{il}/n_l}(\theta_{il})$ is evaluated in the same way as $F_{Z_i/n_i}(z)$ given by Equation (22). N_l' is the number of interferers at SF_l. We have $N_l' = N_l$, if $l \neq i$ and $N_i' = N_i - 1$ for SF_i. The throughput B at the gateway G_0 will then be equal to $M \sum_{i=1}^{K} B_i^M$.

From the above throughput metric, we derive two other metrics to be also applied in orthogonal SF conditions:

- Λ : The total number of packets received at the gateway per end device:

$$\Lambda = M \sum_{i=1}^{K} \frac{B_i^M}{N_i * ToA_i} \tag{26}$$

- P_{succ} : The probability (percentage) of successful transmissions at the gateway that can be approximated by:

$$P_{succ} \approx \frac{B}{M \sum_{i=1}^{K} N i \rho_i^M} = \frac{B}{M * N \rho} \quad (27)$$

where ρ is the average offered load per channel per end device given by $\rho = \sum_{i=1}^{K} \frac{N_i}{N} \rho_i^M$.

V. Numerical Results

In this section, we proceed to the numerical evaluation of the LoRaWAN model presented above under orthogonal and non-orthogonal spreading factor conditions. We adopt the Matlab tool for implementations in conjunction with python scripts. Table III summarizes the main parameters we adopt in our implementations.

TABLE III
Model Parameters

Parameter	Value
Channels' number (M)	3
Carrier frequency (f_c)	868.1 868.2 868.3 Mhz
Emission power (P_0)	14 dbm
Bandwidth (BW)	125 Khz
Path loss exponent (α)	2.7
Coding rate (CR)	$4/5$
Spreading factors	$SF_1 = 7$ to $SF_6 = 12$
Distance Thresholds	l_0=0 km, l_1=3.52 km, l_2=4.86 km, l_3=5.78 km, l_4=6.28 km, l_5=7.15 km, l_6=8.13 km

According to table III, all the nodes transmit at the same power $P_0 = 14\ dbm$ and each device implements the three mandatory channels $[868.1, 868.3, 868.5]$ in the EU 868 MHz ISM band and transmits at a maximum duty cycle $d = 1\%$. Figure 3, depicts the LoRaWAN throughput (in kbps) achieved at G_0 for different deployment scenarios and for different values of the average offered load/channel per end device ρ defined in the previous section. Throughput values are derived under orthogonal and non orthogonal SF conditions and in comparison to the reference pure Aloha throughput.

All the curves in figures 3(a) to 3(d) show that in perfect SF orthogonality conditions, the capture effect that considers the co-SF interferences, allows improving the theoretical throughput achieved by pure Aloha access scheme. Indeed, with pure Aloha, if two signals are transmitted simultaneously, they obviously collide. Whereas, when considering the co-SF interferences, a signal can be decoded at a given spreading factor as long as its strength is higher than the SINR threshold for that SF. Moreover, if we consider the more realistic imperfect SF orthogonality scenario, we notice that throughput values decrease compared to pure Aloha and perfect SF orthogonality conditions.

In figures 3(a) to 3(d) throughput values respectively achieved by the 3 access schemes increase as we increase the offered load/channel ρ. Indeed, for a given number of end devices $N = 300$, and $\rho = 0.5\%$, the throughput values achieved by pure Aloha, Lora with orthogonal SFs and LoRa with non-orthogonal SFs are respectively 2.64 $kbps$, 2.91 $kbps$ and 2.41 $kbps$. These values decrease to 3.14 $kbps$, 3.79 $kbps$ and 2.78 $kbps$ when $\rho = 1\%$ and for same number of EDs. Moreover, we notice that for all these scenarios, the gap between the three access schemes' throughput increases with the number of nodes in the network.

In Figures 3(e) and 3(f), we focus on the throughput variation with the offered load ρ. For the two considered scenarios ($N = 200$ and $N = 600$), throughput values increase until ρ reaches the value of 1% which corresponds to the duty cycle limit per channel defined by the LoRaWAN specifications for the three mandatory channels [868.1,868.3,868.5] MHz. An additional aspect could be noticed in Figure 3(a) where for a small number of nodes ($N = 100$), the throughput obtained in the case of non-orthogonal SFs is higher than the one obtained with pure Aloha. We explain this by the fact that when the number of end devices is small, signals could be decoded even in the presence of concurrent transmissions on other spreading factors as long as the SINR threshold is not reached.

This aspect is further illustrated is Figure 4(a) where we depict the number of the received packets per device at the gateway Vs. the packet generation rate/hour per device λ. Thus for, $N = 100$, $\lambda = 223$ packts/hour and a packet size $= 30\ bytes$, the number of received packets with pure Aloha and LoRa with non-orthogonal SFs are respectively given by 190 pkts/hour and 197 pkts/hour. Whereas, if we increase the packet arrival rate λ to 794 packets/hour (for a packet size $= 10\ bytes$), the number of received packets with pure Aloha is always higher than the one of LoRa with non orthogonal SFs (no matter the number of EDs). For LoRa with orthogonal SFs, however, the number of received packets at the gateway per end device is always higher than Aloha and Lora with non-orthogonal SFs. As in Figure 3(e) and 3(f), Figure 4(c) shows that the number of received packets per device is limited by the duty cycle bound above which it remains unchanged. Figure 4(d), illustrates the variation of the received packets' number with the packet size. We notice that, initially, the number of delivered packets increases with the packet size, then the curves' increase aspect slows down as packet sizes become higher. This is due to the fact that high packet sizes significantly increase the time on air which directly impact the delivered packets' number. As a final step of the LoRaWAN performance evaluation, we depict in Figures 5(a) and 5(b), the probability of successful transmissions. The results in Figures 5(a) and 5(b) corroborate those obtained in previous Figures 4(a) and 4(b) and show that the percentage of successful transmissions reversely decrease with the number of end devices and the traffic load (determined by the packet generation rate and the packet size). This decrease is more significant if the realistic non-orthogonal SF scenario is considered.

For the sake of completeness, we also consider in Table IV different IoT applications [12] for which we characterize the network capacity to achieve high successful transmission probabilities (80% and 90%). From Table IV, we notice

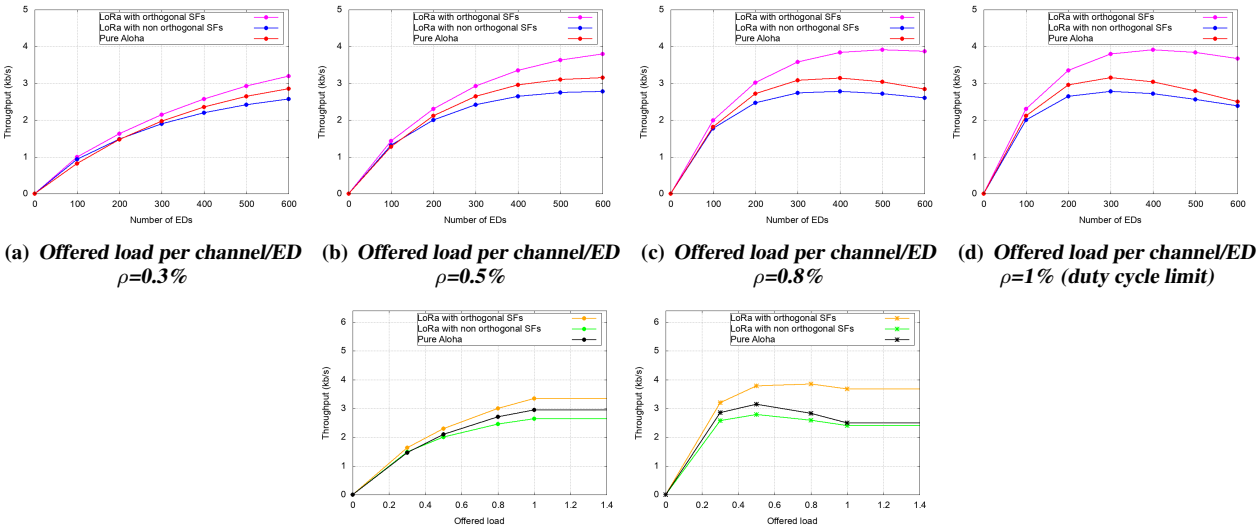

(a) ***Offered load per channel/ED ρ=0.3%*** **(b)** ***Offered load per channel/ED ρ=0.5%*** **(c)** ***Offered load per channel/ED ρ=0.8%*** **(d)** ***Offered load per channel/ED ρ=1% (duty cycle limit)***

(e) ***Throughput Vs. Offered load ρ (ED number=200)*** **(f)** ***Throughput Vs. Offered load ρ (ED number=600)***

Figure 3. LoRaWAN Throughput achieved at the gateway G_0 (kpbs)

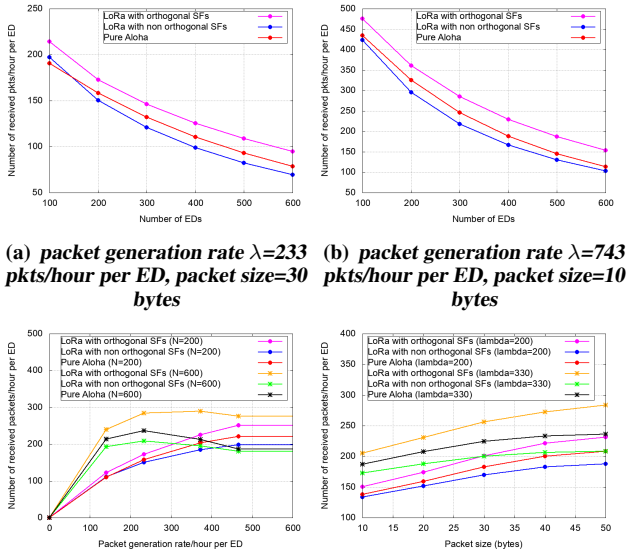

(a) ***packet generation rate λ=233 pkts/hour per ED, packet size=30 bytes*** **(b)** ***packet generation rate λ=743 pkts/hour per ED, packet size=10 bytes***

(c) ***Number of received pkts Vs. packet generation rate λ*** **(d)** ***Number of received pkts Vs. packet size***

Figure 4. Average number of received packets/hour per end device

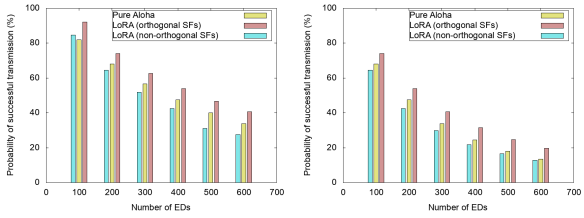

(a) ***packet generation rate λ=233 pkts/hour per ED, packet size=30 bytes*** **(b)** ***packet generation rate λ=743 pkts/hour per ED, packet size=10 bytes***

Figure 5. Probability of successful transmission (%)

that the network capacity depends on the IoT application's characteristics. Thus, for some applications as Roadway signs (where ρ approaches on each channel 50% of the duty cycle), to achieve a high successful transmission percentage (90% for example), the number of end devices under non-orthogonal SFs should not exceed 53 nodes. This number is very small if the IoT application targets the coverage of a whole city. In this context, a multi-gateway deployment would be necessary, as recommended in [11]. Moreover, if pure Aloha or LoRa with orthogonal SFs models are considered to achieve the network dimensioning, this will result in an over estimation of the effective network capacity. As a consequence, the expected percentage of successful transmissions would not be satisfied.

From the above evaluation of LoRaWAN in both orthogonal and non-orthogonal SF conditions and in comparison with pure Aloha, we can conclude that:

- Considering the imperfect SF orthogonality conditions, which are more prone to sustain the real LoRaWAN implementations, has a direct impact on the network performance in terms of achievable throughput at the gateway, the number of delivered packets per end device or the percentage of successful transmissions.
- The LoRaWAN network designer should, imperatively, proceed to the network dimensioning thus to ensure the satisfaction of the expected quality of Service (QoS).
- For some IoT applications, where a certain network density is required to satisfy all the users' needs, a multi-gateway deployment would be preferable to a single cell topology where we are limited by a given number of end devices to achieve a certain QoS.

TABLE IV
LoRaWAN capacity for different IoT applications

IoT Application	Prob. of success (Pure Aloha)		Prob. of success (Lora with orthogonal SFs)		Prob. of success (Lora with non-orthogonal SFs)	
	80%	90%	80%	90%	80%	90%
Roadway signs (message period= 30.03 s, message size= 1 byte)	140	60	180	84	120	53
Traffic lights (message period= 59.88 s, message size= 1 byte)	232	118	320	140	213	99
Credit machine in a shop (message period= 120.48 s, message size= 24 bytes)	276	115	363	154	244	108

VI. Conclusion

In this paper, we focus on the single cell LoRaWAN analysis under unsaturated traffic, multi-channel and duty cycle conditions. We consider both cases of orthogonal and non-orthogonal spreading factors' transmissions. We first, review the background and the work in relation with LoRaWAN performance evaluation. Then, we set the main assumptions at the physical and the network layers we adopt in our analysis. Therefore, we derive the throughput expressions we obtain in perfect and imperfect spreading transmissions. From the throughput, we derive two other performance metrics corresponding to the number of packets delivered per end device and the percentage of successful transmissions. All the results show that considering the imperfect spreading factors' orthogonality in LoRaWAN slows down the network performance in comparison with pure Aloha or a network with perfect SF orthogonality. The imperfect SF orthogonality is a real phenomenon in LoRaWAN and should not be neglected when proceeding to network dimensioning. Moreover, as pure Aloha is adopted at the MAC layer in LoRaWAN, then to satisfy a certain QoS for some IoT applications, the network density show remain relatively low. Thus, a multi-gateway LoRaWAN should be adopted. As a future work, we intend to extend our study to a multi-gateway scenario where capture probabilities should account for gateways' intersection zones.

References

[1] N. Sornin, M. Luis, T. Eirich, T. Kramp, and O. Hersent, *LoRaWAN Specifications 1.0*, Std., 2016.

[2] "Lora modulation basics-an1200.22," Semtech Corporation, Tech. Rep., May 2015.

[3] D. Croce, M. Gucciardo, S. Mangione, G. Santaromita, and I. Tinnirello, "Impact of lora imperfect orthogonality: Analysis of link-level performance," *IEEE Commun. Lett.*, vol. 22, no. 4, 2018.

[4] G. Zhu, C.-H. Liao, M. Suzuki, Y. Narusue, and H. Morikawa, "Evaluation of lora receiver performance under co-technology interference," in *Proc. CCNC*, 2018.

[5] A. Waret, M. Kaneko, A. Guitton, and N. E. Rachkidy, "Lora throughput analysis with imperfect spreading factor orthogonality," in *arXiv:1803.06534v1 [cs.NI]*, 2018.

[6] F. V. den Abeele, J. Haxhibeqiri, I. Moerman, and J. Hoebeke, "Scalability analysis of large-scale lorawan networks in ns-3," *IEEE Internet Things J.*, vol. 4, no. 6, 2017.

[7] D. Magrin, M. Centenaro, and L. Vangelista, "Performance evaluation of lora networks in a smart city scenario," in *Proc. IEEE ICC*, 2017.

[8] M. Bor, J. Vidler, and U. Roedig, "Lora for the internet of things," in *Proc. EWSN '16*, 2016.

[9] J. Petajajarvi, K. Mikhaylov, A. Roivainen, T. Hanninen, and M. Pettissalo, "On the coverage of lpwans: range evaluation and channel attenuation model for lora technology," in *Proc. ITST*, Dec. 2015.

[10] ——, "Evaluation of lora lpwan technology for remote health and wellbeing monitoring," in *Proc. ISMICT*, 2016.

[11] T. V. M. Bor, U. Roedig and J. M. Alonso, "Do lora low-power wide-area networks scale?" in *Proc. ACM MSWIM*, 2016.

[12] K. Mikhaylov, J.Petajajarvi, and T. Hanninen, "Analysis of capacity and scalability of the lora low power wide area network technology," in *Proc. EW'16*, 2016.

[13] R. V. L. Casals, B. Mir and C. Gomez, "Modeling the energy performance of lorawan," *Sensors journal*, October 2017.

[14] F. Delobel, N. E. Rachkidy, and A. Guitton, "Analysis of the delay of confirmed downlink frames in class b of lorawan," in *Proc. VTC Spring'17*, 2017.

[15] F. Adelantado, X. Vilajosana, P. Tuset-Peiro, B. Martinez, J. Melia-Segui, and T. Watteyne, "Understanding the limits of lorawan," *IEEE Commun. Mag.*, vol. 55, no. 9, 2017.

[16] O. Georgiou and U. Raza, "Low power wide area network analysis: Can lora scale?" *IEEE Wireless Commun. Lett.*, vol. 6, no. 2, 2017.

[17] C. Goursaud and J. Gorce, "Dedicated networks for iot: Phy/mac state of the art and challenges," *EAI Endorsed Transactions on Internet of Things*, vol. 1, no. 1, 2015.

[18] V. Gupta, S. K. Devar, N. H. Kumar, and K. P. Bagadi, "Modelling of iot traffic and its impact on lorawan," in *Proc. IEEE Globecom'17*, 2017.

[19] B. Ray, "Improving lorawan scalability," Link Labs, Tech. Rep., January 2017.

[20] R. Borchardt and T. Ha, "Power capture aloha," in *Proc. MILCOM'88*, 1988.

[21] Z. Hadzi-Velkov and B. Spasenovski, "Capture effect in ieee 802.11 basic service area under influence of rayleigh fading and near/far effect," in *Proc. IEEE PIMRC*, 2002.

[22] J. Arnbak and W. van Blitterswijk, "Capacity of slotted aloha in rayleigh-fading channels," *IEEE Sel. Areas Commun.*, vol. 5, no. 2, 1987.

[23] H. S. Chung, D. Skoug, and S. J. Chang, "A fubini theorem for integral transforms and convolution products," *International Journal of Mathematics*, vol. 24, no. 3, 2012.

[24] M. Haenggi, "On routing in random rayleigh fading networks," *IEEE Trans. Wireless Commun.*, vol. 4, no. 4, 2018.